Published in final edited form as:
NMR Biomed. 2011 August ; 24(7): 880–887. doi:10.1002/nbm.1643.

In vivo MRI of early stage mammary cancers and the normal mouse mammary gland

Sanaz A. Jansen[a,†], **Suzanne D. Conzen**[b], **Xiaobing Fan**[a], **Erica Markiewicz**[a], **Thomas Krausz**[c], **Gillian M. Newstead**[a], and **Gregory S. Karczmar**[a,*]

[a] Department of Radiology, University of Chicago, Chicago, IL, USA

[b] Department of Medicine and the Ben May Cancer Center, University of Chicago, Chicago, IL, USA

[c] Department of Pathology, University of Chicago, Chicago, IL, USA

Abstract

Since the advent of screening mammography, approximately one-quarter of newly diagnosed breast cancers are at the earliest preinvasive stage of ductal carcinoma *in situ* (DCIS). Concomitant with this improvement in early detection has been a growing clinical concern that distinguishing aggressive from indolent DCIS is necessary to optimize patient management. Genetically engineered mouse models offer an appealing experimental framework in which to investigate factors that influence and predict progression of preinvasive neoplasias. Because of the small size of early stage carcinomas in mice, high-resolution imaging techniques are required to effectively observe longitudinal progression. The purpose of the present study was to evaluate the feasibility of MRI for assessment of *in situ* mammary neoplasias and early invasive mammary cancers that stochastically arise in mammary glands of C3(1) SV40 Tag transgenic mice. Additionally, images of normal mammary glands from wild-type FVB/N mice were acquired and compared with those from transgenic mice. Sixteen mice underwent MR examinations employing axial two-dimensional multi-slice gradient recalled echo scans (TR/TE=~1000/5.5 ms) with fat suppression in a two-step process targeting both the upper and lower mammary glands. MRI successfully detected *in situ* and early invasive neoplasias in transgenic mice with high sensitivity and specificity. The average signal-to-noise ratio (SNR) of *in situ* lesions on fat-suppressed high-resolution T_1-weighted images was 22.9, which was lower than that of invasive tumors, lymph nodes and muscle (average SNR of 29.5–34.9, $p<0.0001$) but significantly higher than that of normal mammary tissue (average SNR=5.5, $p<0.0001$). Evaluation of wild-type mammary glands revealed no cancerous or benign lesions, and comparable image contrast characteristics (average SNR=5.2) as compared with normal tissue areas of transgenic mice. This present study demonstrates that MRI is an excellent candidate for performing longitudinal assessment of early stage mammary cancer disease progression and response to therapy in the transgenic model system.

* Correspondence to: G. S. Karczmar, University of Chicago, Department of Radiology, 5841 S. Maryland Ave, MC 2026, Chicago, IL 60637, USA.
† Present address: Mouse Cancer Genetics Program, National Cancer Institute, Frederick, MD, USA.

Keywords

MRI; ductal carcinoma *in situ*; mouse models; mammary intraepithelial neoplasia; mammary gland; imaging

INTRODUCTION

As a result of the widespread use of screening mammography in the US approximately 60% (1) of breast cancers are diagnosed at an early stage, specifically, as small invasive ductal carcinoma (IDC) or its preinvasive nonobligate precursor ductal carcinoma *in situ* (DCIS) (2). The large proportion of early stage cancers and the excellent prognosis for many patients in this group (3) puts breast cancer in a relatively uncommon position among malignancies: important directions for future research lie not only in achieving further improvements in detection and treatment, but also in avoiding overdiagnosis and overtreatment of possibly indolent lesions (4), of particular concern for DCIS (5,6). Recent reports outlining top translational breast cancer research priorities (7,8) included understanding the factors that lead to progression of DCIS, with an eventual clinical goal of identifying those patients at high risk of subsequent invasive events and requiring intervention compared with those low-risk patients who may benefit from less aggressive treatment. Thus, determining the optimal management of early stage breast cancers is an area of intense research (9–12) directed at discovering the molecular, genetic or radiologic features that can stratify patients and tailor subsequent interventions accordingly.

Transgenic mouse models provide an important framework for such research in a preclinical setting. Mouse models allow for a longitudinal assessment of disease development and progression that is challenging to perform in women and is crucial for studies of treatment response, chemoprevention and factors that influence progression of early stage malignancies. To date, most preclinical longitudinal experiments use calipers to measure changes in palpable tumor volume over time (13,14). The advantage of this technique is that it is a quick and simple measurement; the disadvantage is that palpable tumors are not adequate models of early breast cancer. Early stage murine mammary cancers are too small to be visible or palpable and thus *in vivo* imaging methods are required to assess longitudinal progression. However, relatively few previous reports have explored such imaging strategies (15–17). In particular, what is currently lacking is a minimally invasive screening examination that can quickly and reliably identify *in situ* and early invasive malignancies stochastically arising in any of the 10 mouse mammary glands, and accurately assess tumor morphology and volume over time.

In previous studies we developed MRI techniques to detect early stage murine mammary cancer with high sensitivity (17). While these techniques illustrated the potential for MRI to be a valuable tool for preclinical studies of early breast cancer, they would not be suitable as a screening examination as they could only be used to image two out of ten mammary glands using specialized instrumentation. Because mouse mammary glands span the length of the mouse on both sides, images of the entire mouse body are necessary to capture all glands. At the same time, very high-spatial resolution and a signal-to-noise ratio (SNR) are

required to detect and evaluate very small intra-ductal cancers. Thus, the purpose of present study was to evaluate the feasibility of whole-body screening MRI for assessment of early stage mammary cancers. The C3(1) SV40 Tag transgenic mouse model was utilized wherein preinvasive cancers stochastically arise and progress to invasive tumors; additionally, wild-type FVB/N mice were selected to compare with the cancerous glands. Mice were imaged in a volume coil allowing for whole-body imaging in a two-step process using T_1-weighting with fat suppression at both high- and low-spatial resolution. Images were correlated with histology to measure the sensitivity of each technique for detection of early stage malignancies. Additionally, the MR presentation of normal tissue, preinvasive and invasive cancers was compared using the SNR and contrast-to-noise ratio (CNR) in this first reported comparison of MRI of the normal and early stage malignant mouse mammary gland.

EXPERIMENTAL

Animals

All procedures were carried out in accordance with our institution's Animal Care and Use Committee approval. A total of 16 mice were used in this present study for imaging experiments, including eight C3(1) SV40 large T-antigen (Tag) transgenic mice (on a FVB/N background) and eight FVB/N wild-type mice (Harlan Laboratories, Inc., Indianapolis, IN, USA). In the C3(1) SV40 Tag mouse model (18) of breast cancer, at ~8 weeks of age female mice develop atypical ductal hyperplasia, and at ~12 weeks mammary intraepithelial neoplasia (MIN) (19). These MIN lesions exhibit several similarities to human DCIS, as they represent neoplastic cells confined by the duct basement membrane that are thought to be precursors to an invasive tumor (20), although they may not reflect all histolopathologic subtypes of their human counterpart (21). Invasive tumors develop at ~16 weeks of age. The age of transgenic and wild-type mice imaged ranged from 12 to 17 weeks and 12 to 15 weeks, respectively. Animals were anesthetized before imaging experiments, and anesthesia was maintained during imaging at 1.5% isoflorane. The temperature, heart rate and respiration rate were monitored with data taken every minute, and the respiration rate was used to obtain gated images.

Six out of ten mouse mammary glands (the right and left cervical and thoracic glands) are located in the upper half of the mouse, towards the head; we will refer to these six glands as the upper glands (22). The remaining four mammary glands (the right and left abdominal and inguinal glands) are located in the lower half of the mouse towards the tail; we will refer to these four glands as the lower glands. Thus, each mouse has a total of ten individual mammary glands which in our terminology is equivalent to a total of four sets of glands: right upper, left upper, right lower and left lower.

Imaging techniques and histologic correlation

Imaging was performed on a 30-cm horizontal bore Bruker BioSpec 9.4 Tesla Small Animal MR System (Bruker-Biospin, Billerica, MA) with a maximum gradient strength of 300 mT/m. Two whole-body screening MRI protocols were evaluated, one at high-spatial resolution and the other at lower spatial resolution, specifically at half the in-plane spatial resolution and double the slice thickness of the high-resolution scan, with half the imaging

time. As detailed below, the sensitivity of each imaging protocol for early stage murine mammary cancers was compared by performing histologic correlation. In addition, the SNR and CNR were quantified for early stage mammary cancers in the transgenic mice as well as normal tissue in both transgenic and wild-type FVB/N mammary glands.

Eight C3(1) SV40 Tag transgenic mice were selected for whole-body screening examinations employing both high (slice thickness=0.5 mm, in plane resolution=117 μm) and low (slice thickness=1.0 mm, in plane resolution=234 μm) spatial resolution axial two-dimensional multi-slice gated gradient recalled echo (GRE) scans with spectrally selective fat suppression and modest T_1-weighting (TR/TE=~1000/5.5 ms, field of view=30×30 mm, flip angle=30°, number of excitations=2). Mice were taped into a plastic semi-circular holder and placed inside a volume quad coil (Bruker BioSpin MRI GmbH Quad coil, OD/ID=59/35mm, length=38mm). Lower and upper mammary glands on both sides were scanned in a two-step process, with the upper region imaged first followed by imaging of the lower region after pulling the mouse out of the magnet by 40 mm. A range of 84–148 slices for high resolution and 42–74 slices for low resolution images were required to cover all glands. If run separately, the approximate imaging time (i.e. total time the mouse would be in the magnet) for high- and low-resolution whole-body screening MRI is approximately 30 and 15 min, respectively; in the present study these scans were run consecutively with a total imaging time of approximately 40 min. Eight FVB/N wild-type mice were selected for high- and low-spatial resolution screening MRI scans of the lower mammary gland region (using the second step of the whole-body screening protocols outlined above).

To facilitate correlation of MR images with histology, a fine polyethylene mesh ~ 40×20 mm in size with 3.0-mm spacing was embedded in partially deuterated agar and wrapped around each mouse during imaging. Using a Sharpie marker, the grid position was marked on the skin of the mouse. This grid produced a pattern on MRI that in previous work has allowed for registration of serial MR images so that lesions could be located and followed over time (23) and also for correlation of images with histology (17). After imaging, mice were euthanized and mammary glands excised and fixed in 10% formalin over night. In a total of ten mice (six transgenic and four wild type) hematoxylin and eosin (H&E)-stained sections of imaged mammary glands were obtained (5-micron thick H&E sections every 50 microns) and evaluated by a pathologist (T.K.) with over 20 years of experience in the evaluation of breast and mouse mammary glands.

Image analysis

All data analysis was performed using homemade software written in IDL (Research Systems, Inc., Boulder, CO) by a postdoctoral fellow (S.A.J.) with 5 years of experience analyzing MR images of early murine mammary cancers. Initially, the sensitivity of the low and high-spatial resolution screening MR protocols for detection of early cancerous lesions was calculated by performing a region-based analysis of the MR images of C3(1) SV40 Tag mice and the corresponding histology. As detailed in previous work (23), lower and upper mammary glands were divided into three regions and each identified as normal, preinvasive (MIN only) or invasive (at least one invasive tumor with or without MIN) based on the pathologists classification. MR images were reviewed separately and mammary gland

regions classified into the same categories based on use of morphologic criteria to identify MIN, invasive tumors and lymph nodes [presenting as nonmass, mass and lobulated lesions, respectively, as described in (17)]. MR images were correlated with H&E sections using the agar grid as in previous work (17) and sensitivity of MRI was calculated using the pathologic evaluation as the reference standard. The high-resolution MR images were analyzed by the same reader (S.A.J.) 1 month after the low-resolution MR images, and were interpreted blinded to the low-resolution findings.

Subsequent to this detailed region-based analysis within glands, a more global gland-based analysis of C3(1) SV40 Tag mice was performed in all eight mice to assess variation in cancer burden in upper vs. lower mammary glands based on their imaging characteristics. Previous reports and experience with this mouse model have shown an increased incidence of mammary tumors in the upper glands and more rapid tumor progression (24), although the mechanism underlying this difference is not fully understood. To assess the variation in cancer burden in the same mouse, entire lower and upper glands were individually classified as normal (no cancerous disease evident), preinvasive (MIN only) and invasive (at least one invasive tumor) based on their MR imaging characteristics, using morphologic criteria outlined above. Malignant glands were further categorized as unifocal (one single invasive mass) or multifocal (several distinct invasive masses). The size of the largest invasive tumor was measured and compared with lower and upper glands using the Mann–Whitney rank-and-sum test with a p-value<0.05 indicating significance.

Finally, the MRI characteristics of early mammary cancers and normal tissue were quantified. The following regions of interest (ROI) were manually traced, guided by the histologic evaluation using the region-based analysis detailed above, or the lesion morphology: early invasive cancer, MIN, lymph node, normal mammary gland (NMG) and muscle. The SNR of these regions was calculated separately for the high- and low-resolution screening MRI examinations as follows:

$$SNR = \bar{S} / \sigma_{noise}$$

where $\bar{S}$ is the average signal intensity in the ROI and σ_{noise} was averaged from the standard deviations of signal intensities measured in a 5×5 mm ROI drawn in the corners of the modulus images. In addition, the CNR of these ROIs was calculated relative to NMG tissue as follows:

$$CNR_{ROI-NMG} = SNR_{ROI} - SNR_{NMG}.$$

The Mann–Whitney test was used to compare (i) the SNR and CNR_{NMG} of MIN, invasive tumors, lymph nodes, muscle and normal tissue in transgenic mice, (ii) the SNR of normal tissue, lymph nodes and muscle in transgenic vs. wild-type mice and (iii) the size of lymph nodes in transgenic vs. wild-type mice. For all tests, a p-value<0.05 was selected to indicate significance.

RESULTS

Screening MRI of transgenic mammary glands

Whole-body screening MR images detected early carcinomas in the upper and lower mammary glands of transgenic mice with high sensitivity. Examples of images from one mouse are shown in Fig. 1, where axial high spatial resolution screening MR images from all inguinal glands were obtained, demonstrating that MIN, early invasive tumors and lymph nodes appeared clearly against a darker background of normal tissue in fat-suppressed images. Region-based analysis within glands was used to compare histologic evaluation with image-based assessments of lesion pathology in six mice. High resolution imaging correctly identified six out of six lymph nodes, 16 out of 16 regions with invasive cancer and nine out of nine regions containing preinvasive cancers. In comparison, low resolution imaging correctly identified six lymph nodes, 14 invasive regions and six preinvasive regions. Figure 2 demonstrates that some MIN regions visualized on high spatial resolution scans are not well visualized on low spatial resolution images.

In addition to performing this region-based assessment of cancerous disease extent within each set of glands, a global assessment of lower and upper glands was performed to categorize them as normal, preinvasive or invasive based on high-resolution screening MRI characteristics. This analysis revealed considerable differences in cancer burden between the lower and upper glands (Table 1). The majority (10/16) of the lower glands were classified as normal or preinvasive compared with less than one-fifth (3/16) of the upper glands. The upper glands were not only more likely to be classified as malignant compared with the lower glands, but their invasive cancers were more aggressive: 62% (8/13) of malignant upper glands were classified as multifocal, compared with 33% (2/6) of malignant lower glands. The largest invasive tumors in the upper glands measured 4.1±2.1 mm on average (range 1.5–8.7 mm), which was larger than their counterparts in the lower glands at 3.1±1.9 mm (range 1.7–6.9 mm), although this difference was not statistically significant ($p>0.3$). All mice with invasive tumors in the lower glands had larger invasive tumors in their upper glands.

To quantify the presentation of early cancers and other regions of interest, the SNR and CNR_{NMG} were calculated. The SNR of MIN was significantly lower than that of invasive tumors, lymph nodes and muscle ($p<0.0001$) (Fig. 3). On the other hand, invasive tumors exhibited similar SNR compared with muscle ($p>0.2$) and slightly lower SNR than lymph nodes ($p<0.02$). All including MIN had much larger SNR compared with NMG ($p<0.0001$), which was reflected in the high CNR_{NMG} values. As expected, SNR was overall increased in the low compared with high-resolution screening MRI scans.

Screening MRI of wild-type mammary glands

Low and high-spatial resolution screening MRI examinations of the inguinal glands of wild-type FVB/N mice was performed and compared with histology. None of the H&E sections demonstrated any cancerous or benign lesions at any age examined. Qualitative examination of the histologic sections found that age-matched wild-type FVB/N nontransgenic mice exhibited a more tortuous and dense ductal branching pattern compared with noncancerous

regions of the transgenic C3(1) SV40 Tag FVB/N mice. The SNR of muscle and NMG was similar in the FVB/N as in the transgenic mice ($p>0.1$) (Fig. 3). Lymph nodes in FVB/N mice had a slightly lower SNR compared with C3(1) SV40 Tag mice ($p=0.01$), but were observed to be similar in size at 1.8±0.3 mm and 1.8±0.2 mm for FVB/N and C3(1) SV40 Tag mice, respectively. Review of the MR images showed that in eight out of nine FVB/N wild-type mice, high resolution screening MRI scans detected faint segmental nonmass structures near the lymph node that were determined to be large blood vessels by histologic correlation (Fig. 4). The SNR of these blood vessels detected in wild-type FVB/N mice was lower than that of the MIN lesions detected in C3(1) SV40 Tag mice at 17.3±3.1 compared with 22.9±5.0, respectively ($p<0.0006$). Only two of nine low resolution scans detected the same structures.

DISCUSSION

Transgenic mouse models of breast cancer provide an appealing experimental framework in which to design and evaluate new strategies for improving the detection, treatment and prevention of breast cancer. This is in part due to the fact that longitudinal disease progression can be monitored in mice in a way that is essentially impossible to do in women. To improve the relevance and efficacy of such longitudinal studies, there is a need for a rapid, reliable and inexpensive assessment of the full range of cancer initiation and progression, from *in situ* to early invasive to advanced disease. In the present study, we have demonstrated that screening MRI is an excellent tool for this purpose.

We have previously shown that MR imaging could detect the earliest stages of mammary cancer in transgenic mice, using a specialized home-built half-open birdcage coil (17,23,25,26) that could only target two mammary glands on only one side of the mouse. We used these techniques to perform a pilot study of the progression of MIN lesions that developed in the left lower (inguinal and abdominal) mammary glands of C3(1) SV40 Tag mice, with results suggesting MIN lesions may progress, regress or remain indolent in this model (23). The advantage of the whole-body screening MRI protocols presented in the present study is that a widely accessible commercially available coil was used and that images from all mammary glands were obtained, so that the timescales of development and progression of early murine mammary cancers can be evaluated in both lower and upper mammary glands on both sides of the animal. This is an important capability, as previous reports have shown that in this and other mouse models tumorigenesis is accelerated in upper glands (27,28); in our current image-based analysis, we too found that upper glands exhibited a higher proportion of invasive, multifocal tumors compared with lower glands. Furthermore, we found that high spatial resolution whole-body screening MRI demonstrated high accuracy in identifying the earliest stages of mammary cancer in the C3(1) SV40 Tag model, and exhibited comparable sensitivity, qualitative and quantitative lesion features as compared with our previous study (17) using a dedicated mammary gland examination. We have also tested a faster (~15 min) lower spatial resolution screening MRI examination, which can still successfully detect a majority of preinvasive and invasive cancerous regions, although with less morphologic detail.

The cost of MRI is a possible limitation for studying mouse models. However, because of its capacity for noninvasive identification of preinvasive and nonpalpable invasive cancers without euthanization fewer mice would be needed in longitudinal studies, and fewer mammary glands would require expensive and time-consuming histologic evaluation. In addition, the present results demonstrate that a screening examination of all mammary glands can be completed in 30 min or less, and thus would be relatively inexpensive. The main limitations of screening MRI are the potential for false positives and false negatives, although as the most sensitive currently available *in vivo* technique, MRI is the least susceptible to the latter concern. Our results examining the characteristics of normal glands in wild-type mice suggest that near the lymph node it is possible for blood vessels to be mistaken for small *in situ* carcinomas on some screening MRI examinations giving rise to potential false positives, although it is important to note that we have not encountered false positives in our investigations of the C3(1) SV40 Tag mouse model thus far. It is also possible that some MIN and invasive tumors may be mistaken for one another based on their image-based characteristics, particularly for small focal lesions, although this has not been common in our experience. A larger sensitivity/specificity study is required to correlate a wide range of image-based characteristics with the underlying pathology; more generally it will be important to devise strategies in mice to minimize false positives to ensure reliable identification of preinvasive and invasive regions. Such strategies will probably involve extending the purely anatomic imaging techniques used in the present study by incorporating functional imaging methods and other types of contrast. For example, blood vessels could perhaps be distinguished from the MIN lesions they resemble on the noncontrast images presented herein by using dynamic contrast enhanced MRI or MR angiographic methods to assess flow.

The mechanisms underlying the observed endogenous contrast between the normal mammary gland and early murine mammary cancers are not clear, especially considering that clinical breast MRI protocols involve the injection of a gadolinium chelate for lesion visualization in women. Conspicuity of *in situ* and early invasive tumors may reflect large variations compared with normal tissue of relaxation parameters T_1, T^{2*} as well as proton density, where the phrase ‘proton density’ is used to refer to water protons that are detectable by MRI using standard imaging parameters (as opposed to solid-state MRI methods). It may also be because of partial volume effects; in the normal mouse mammary gland, the ductal tree is diffusely distributed within the mammary fat pad and individual ducts/lobules are rarely resolved. Therefore ROIs drawn around normal mammary glands almost certainly contain some regions of suppressed fat thus reducing the overall average signal intensity. It should be emphasized that the SNR and CNR measurements reported here are specific for the very modestly T_1 weighted, fat-suppressed images acquired in the present study. More work is needed to quantify T_1, proton density, as well as other MRI parameters in mouse mammary glands.

The *in vivo* imaging characteristics of the normal mouse mammary gland are rarely studied (26); in the present study we have compared normal tissue in transgenic vs. wild-type mice of the same background. No cancerous or benign lesions developed in the wild-type mice examined. We found that the SNR of normal tissue areas after fat suppression were similar

in both strains of mice, while lymph nodes exhibited slightly lower signal intensity in wild-type compared with transgenic mice. Interestingly, histologic evaluation of the mammary glands demonstrated qualitative differences in duct density and morphology between transgenic and wild-type mice included in our study. This anecdotal observation is concordant with previous studies that found differences in ductal branching patterns in strains of wild-type mice at increased risk for developing spontaneous mammary tumors compared with those strains with a lower risk (29). To find image-based features that can capture these and other disparities, further work should be performed to use additional MRI-based imaging methods, including quantitative relaxometry and functional MRI methods such as dynamic contrast enhanced MR imaging (26), to correlate with the underlying physiology and anatomy of the normal mammary gland. Although differences between the normal mouse and human mammary gland are significant (30), the possibility for using mice to develop and validate image-based assessments of cancer risk is an important topic for further exploration.

There are several limitations to this study. First, errors may have been made while correlating MR images with histology, as a result of distortions in the excision and fixation process as well as misregistration of the agar-grid technique. Incorrect histologic correlation would adversely affect sensitivity calculations as well as ROI placement for SNR calculations. Second, as alluded to earlier, performing lesion classification (as MIN or invasive) based on MR presentation may be inaccurate in some cases, although our previous work has suggested that morphologic descriptors are highly predictive of histologic status. A larger sensitivity and specificity study with improved lesion feature analysis is necessary to improve MR-based lesion identification. If MRI is to be used in longitudinal studies of early mammary cancer progression, the capacity for image-based features to represent the true lesion histopathology must be maximized. Finally, we did not employ contrast enhanced imaging techniques in the current study, and instead focused on establishing the efficacy of noncontrast imaging techniques. This limits the translation of our results to the clinical breast imaging setting wherein clinical protocols utilize dynamic contrast enhanced MR imaging protocols (31) for visualization of breast neoplasms.

To summarize, we have used noninvasive *in vivo* imaging to characterize the normal mammary gland in wild-type vs. transgenic mice, and the preinvasive and invasive malignant mammary gland in transgenic mice. We have demonstrated that MR imaging can be used to provide a rapid assessment of early cancerous disease extent in all mouse mammary glands, and is thus an excellent candidate for performing longitudinal assessment of mammary cancer disease progression and response to therapy. To our knowledge the approach presented herein is the only imaging strategy that can provide three-dimensional, high-resolution *in vivo* images of stochastically arising *in situ* and early invasive lesion morphology and tumor volume. Future work can expand on these predominantly anatomic imaging protocols, for example using dynamic contrast enhanced and diffusion weighted MRI to assess lesion vasculature, physiology and cellularity. Other imaging modalities, such as positron emission tomography (PET) of tissue metabolism, could also be used in conjunction with MRI to provide additional lesion characterization (15,16). By using multimodality *in vivo* imaging techniques to interrogate the dynamics of early

tumorigenesis, i.e. how lesion characteristics change over time, it may be possible to find image-based biomarkers that are predictive of progression. Such biomarkers could be used along with other clinical and biological features to distinguish indolent from aggressive cancers and help determine the optimal clinical management of patients diagnosed with early breast cancer.

Acknowledgments

We would like to thank the Segal Foundation, NIH grant P50 CA125183-01 (SPORE) and The University of Chicago Cancer Center for financial support.

Abbreviations

C3(1)	rat prostatic steroid binding protein gene
CNR	contrast-to-noise ratio
DCIS	ductal carcinoma in situ
FVB/N	friend virus B NIH
GRE	gradient recalled echo
FOV	field of view
H&E	hematoxylin and eosin
IDC	invasive ductal carcinoma
MIN	mammary intraepithelial neoplasia
NMG	normal mammary gland
ROI	regions of interest
SNR	signal-to-noise ratio
SV40	Simian virus 40
Tag	large tumor antigen
TE	time to echo
TR	repetition time

REFERENCES

1. Altekruse, SF.; Kosary, CL.; Krapcho, M.; Neyman, N.; Aminou, RWW.; Ruhl, J.; Howlader, N.; Tatalovich, Z.; Cho, H.; Mariotto, A.; Eisner, MP.; Lewis, DR.; Cronin, K.; Chen, HS.; Feuer, EJ.; Stinchcomb, DG.; Edwards, BK. SEER Cancer Statistics Review, 1975-2007. National Cancer Institute; Bethesda, MD: 2009.
2. American Cancer Society. Breast Cancer Facts & Figures 2009-2010. American Cancer Society, Inc.;
3. Gloeckler Ries LA, Reichman ME, Lewis DR, Hankey BF, Edwards BK. Cancer survival and incidence from the Surveillance, Epidemiology, and End Results (SEER) program. Oncologist. 2003; 8:541–552. [PubMed: 14657533]
4. Benson JR, Jatoi I, Keisch M, Esteva FJ, Makris A, Jordan VC. Early breast cancer. Lancet. 2009; 373:1463–1479. [PubMed: 19394537]

5. Allegra CJ, Aberle DR, Ganschow P, Hahn SM, Lee CN, Millon-Underwood S, Pike MC, Reed SD, Saftlas AF, Scarvalone SA, Schwartz AM, Slomski C, Yothers G, Zon R. National Institutes of Health State-of-the-Science Conference statement: diagnosis and management of ductal carcinoma in situ. J. Natl. Cancer Inst. 2009; 102:161–169. [PubMed: 20071686]

6. Erbas B, Provenzano E, Armes J, Gertig D. The natural history of ductal carcinoma in situ of the breast: a review. Breast Cancer Res. Treat. 2006; 97:135–144. [PubMed: 16319971]

7. Dowsett M, Goldhirsch A, Hayes DF, Senn HJ, Wood W, Viale G. International Web-based consultation on priorities for translational breast cancer research. Breast Cancer Res. 2007; 9:R81. [PubMed: 18034879]

8. Thompson A, Brennan K, Cox A, Gee J, Harcourt D, Harris A, Harvie M, Holen I, Howell A, Nicholson R, Steel M, Streuli C. Evaluation of the current knowledge limitations in breast cancer research: a gap analysis. Breast Cancer Res. 2008; 10:R26. [PubMed: 18371194]

9. Llombart-Cussac A. Improving decision-making in early breast cancer: who to treat and how? Breast Cancer Res. Treat. 2008; 112(Suppl 1):15–24. [PubMed: 19082929]

10. Pawitan Y, Bjohle J, Amler L, Borg AL, Egyhazi S, Hall P, Han X, Holmberg L, Huang F, Klaar S, Liu ET, Miller L, Nordgren H, Ploner A, Sandelin K, Shaw PM, Smeds J, Skoog L, Wedren S, Bergh J. Gene expression profiling spares early breast cancer patients from adjuvant therapy: derived and validated in two population-based cohorts. Breast Cancer Res. 2005; 7:R953–964. [PubMed: 16280042]

11. Bedard PL, Di Leo A, Piccart-Gebhart MJ. Taxanes: optimizing adjuvant chemotherapy for early-stage breast cancer. Nat. Rev. Clin. Oncol. 2010; 7:22–36. [PubMed: 19997076]

12. Kesisis G, Makris A, Miles D. Update on the use of aromatase inhibitors in early-stage breast cancer. Breast Cancer Res. 2009; 11:211. [PubMed: 19889200]

13. Dey JH, Bianchi F, Voshol J, Bonenfant D, Oakeley EJ, Hynes NE. Targeting flbroblast growth factor receptors blocks PI3K/AKT signaling, induces apoptosis, and impairs mammary tumor outgrowth and metastasis. Cancer Res. 2010; 70:4151–4162. [PubMed: 20460524]

14. Lu Y, Bertran S, Samuels TA, Mira YLR, Farias EF. Mechanism of inhibition of MMTV-neu and MMTV-wnt1 induced mammary oncogenesis by RARalpha agonist AM580. Oncogene. 2010; 29:3665–3676. [PubMed: 20453882]

15. Abbey CK, Borowsky AD, Gregg JP, Cardiff RD, Cherry SR. Preclinical imaging of mammary intraepithelial neoplasia with positron emission tomography. J. Mammary Gland. Biol. Neoplasia. 2006; 11:137–149. [PubMed: 17091397]

16. Abbey CK, Borowsky AD, McGoldrick ET, Gregg JP, Maglione JE, Cardiff RD, Cherry SR. In vivo positron-emission tomography imaging of progression and transformation in a mouse model of mammary neoplasia. Proc. Natl. Acad. Sci. U.S.A. 2004; 101:11438–11443. [PubMed: 15277673]

17. Jansen SA, Conzen SD, Fan X, Krausz T, Zamora M, Foxley S, River J, Newstead GM, Karczmar GS. Detection of in situ mammary cancer in a transgenic mouse model: in vitro and in vivo MRI studies demonstrate histopathologic correlation. Phys. Med. Biol. 2008; 53:5481–5493. [PubMed: 18780960]

18. Maroulakou IG, Anver M, Garrett L, Green JE. Prostate and mammary adenocarcinoma in transgenic mice carrying a rat C3(1) simian virus 40 large tumor antigen fusion gene. Proc. Natl. Acad. Sci. U.S.A. 1994; 91:11236–11240. [PubMed: 7972041]

19. Cardiff RD, Anver MR, Gusterson BA, Hennighausen L, Jensen RA, Merino MJ, Rehm S, Russo J, Tavassoli FA, Wakefield LM, Ward JM, Green JE. The mammary pathology of genetically engineered mice: the consensus report and recommendations from the Annapolis meeting. Oncogene. 2000; 19:968–988. [PubMed: 10713680]

20. Green JE, Shibata MA, Yoshidome K, Liu ML, Jorcyk C, Anver MR, Wigginton J, Wiltrout R, Shibata E, Kaczmarczyk S, Wang W, Liu ZY, Calvo A, Couldrey C. The C3(1)/SV40 T-antigen transgenic mouse model of mammary cancer: ductal epithelial cell targeting with multistage progression to carcinoma. Oncogene. 2000; 19:1020–1027. [PubMed: 10713685]

21. Frech MS, Halama ED, Tilli MT, Singh B, Gunther EJ, Chodosh LA, Flaws JA, Furth PA. Deregulated estrogen receptor alpha expression in mammary epithelial cells of transgenic mice

results in the development of ductal carcinoma in situ. Cancer Res. 2005; 65:681–685. [PubMed: 15705859]

22. Cardiff, RD. Mammary Cancer in Humans and Mice: A Tutorial for Comparative Pathology. Dec 30. 2010 http://www.compmed.ucdavis.edu/bcancercd/ Date accessed:
23. Jansen SA, Conzen SD, Fan X, Markiewicz EJ, Newstead GM, Karczmar GS. Magnetic resonance imaging of the natural history of in situ mammary neoplasia in transgenic mice: a pilot study. Breast Cancer Res. 2009; 11:R65. [PubMed: 19732414]
24. Green JE, Shibata MA, Shibata E, Moon RC, Anver MR, Kelloff G, Lubet R. 2-difluoromethylornithine and dehydroepiandrosterone inhibit mammary tumor progression but not mammary or prostate tumor initiation in C3(1)/SV40 T/t-antigen transgenic mice. Cancer Res. 2001; 61:7449–7455. [PubMed: 11606379]
25. Fan X, Markiewicz EJ, Zamora M, Karczmar GS, Roman BB. Comparison and evaluation of mouse cardiac MRI acquired with open birdcage, single loop surface and volume birdcage coils. Phys. Med. Biol. 2006; 51:N451–459. [PubMed: 17148815]
26. Jansen SA, Paunesku T, Fan X, Woloschak GE, Vogt S, Conzen SD, Krausz T, Newstead GM, Karczmar GS. Ductal carcinoma in situ: X-ray fluorescence microscopy and dynamic contrast-enhanced MR imaging reveals gadolinium uptake within neoplastic mammary ducts in a murine model. Radiology. 2009; 253:399–406. [PubMed: 19864527]
27. Bolander FF Jr. Differential characteristics of the thoracic and abdominal mammary glands from mice. Exp. Cell. Res. 1990; 189:142–144. [PubMed: 2189737]
28. Sheldon WG, Owen K, Weed L, Kodell R. Distribution of mammary gland neoplasms and factors influencing metastases in hybrid mice. Lab. Anim. Sci. 1982; 32:166–168. [PubMed: 7078083]
29. Naylor MJ, Ormandy CJ. Mouse strain-specific patterns of mammary epithelial ductal side branching are elicited by stromal factors. Dev. Dyn. 2002; 225:100–105. [PubMed: 12203726]
30. Cardiff RD, Wellings SR. The comparative pathology of human and mouse mammary glands. J. Mammary Gland. Biol. Neoplasia. 1999; 4:105–122. [PubMed: 10219910]
31. Schnall MD, Blume J, Bluemke DA, DeAngelis GA, DeBruhl N, Harms S, Heywang-Kobrunner SH, Hylton N, Kuhl CK, Pisano ED, Causer P, Schnitt SJ, Thickman D, Stelling CB, Weatherall PT, Lehman C, Gatsonis CA. Diagnostic architectural and dynamic features at breast MR imaging: multicenter study. Radiology. 2006; 238:42–53. [PubMed: 16373758]

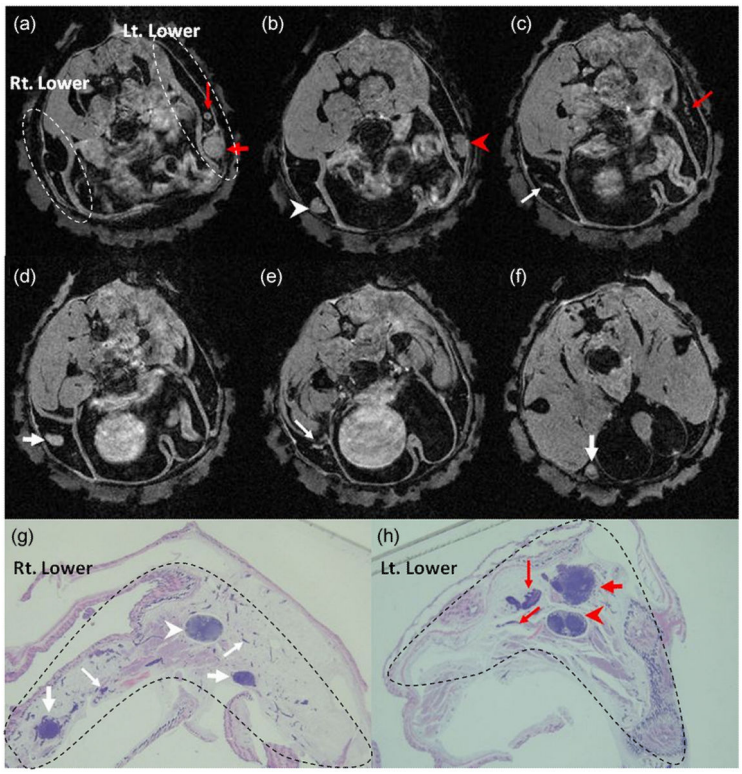

Figure 1.

High-resolution axial screening MR images (a–f) and corresponding histologic sections (g–h) of right (white arrows) and left (red arrows) lower mammary glands from one C3(1) SV40 Tag mouse. Each axial MR image represents only one cross sectional slice through the right and left lower glands, as indicated in (a) by the dashed outlines. Conversely, histologic sections represent the entire glands, as indicated in (g–h) by the dashed outlines. The agar grid, which can be visualized wrapped around the mouse, helps to facilitate correlation of MR images with histology. MR images demonstrate lymph nodes (arrowheads), invasive tumors (thick arrows) and MIN (thin arrows). FOV for MR images is ~ 2.25×2.25 cm.

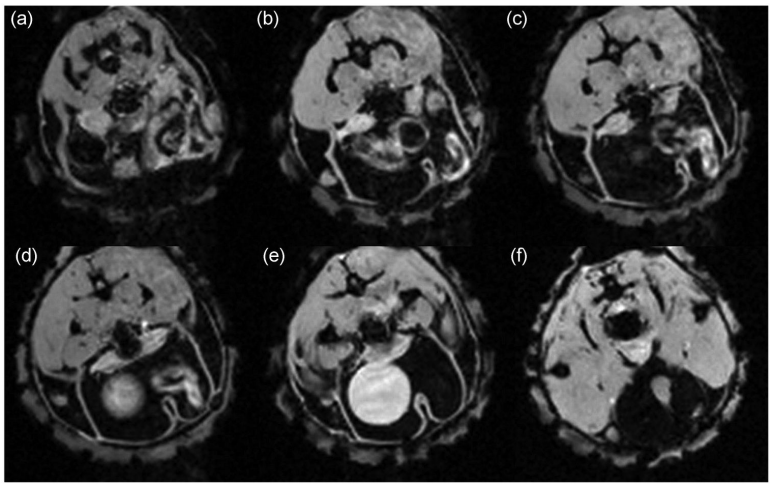

Figure 2.

Low-resolution screening MR images of similar slices as shown in Fig. 1. MIN lesions identified in Fig. 1C are not as well visualized on lower resolution scans. FOV is ~ 2.25×2.25 cm.

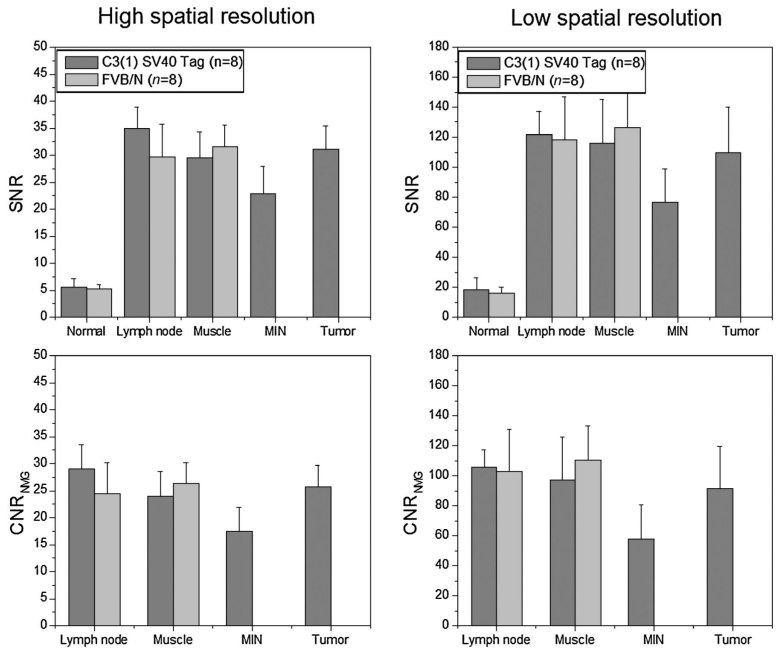

Figure 3.

SNR and CNR_{NMG} of various ROIs for both the high- and low-resolution screening MRI scans in C3(1) SV40 Tag transgenic mice (dark gray) and the FVB wild-type mice (light gray). MIN lesions exhibited significantly lower SNR and CNR_{NMG} compared with lymph nodes, muscle and tumors. Normal mammary tissue in transgenic and wild-type mice exhibited a similar SNR.

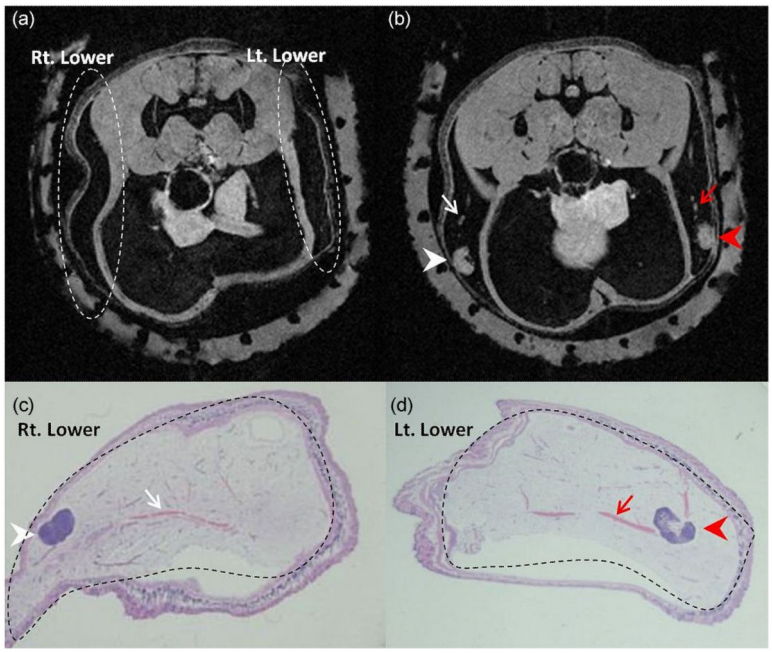

Figure 4.

High-resolution axial screening MR images (a–b) and corresponding histologic sections (c–d) of right (white arrows) and left (red arrows) lower mammary glands from one wild-type FVB/N mouse. Each axial MR image represents only one cross sectional slice through the right and left lower glands, as indicated in (a) by the dashed outlines. Conversely, histologic sections represent the entire glands, as indicated in (c–d) by the dashed outlines. The agar grid, which can be visualized wrapped around the mouse, helps to facilitate correlation of MR images with histology. MR images demonstrate (a) normal mammary gland with no lesion or lymph node, (b) lymph nodes (arrowheads) and large blood vessels (thin arrows). FOV for MR images is ~ 2.25×2.25 cm.

Table 1

Classification of glands as normal, preinvasive and invasive based on MRI characteristics in a total of 32 sets of mamnnary glands (16 upper, 16 lower) from eight C3(1) SV40 Tag mice.

				Invasive	
	Lymph Nodes	**Normal**	**Preinvasive**	**Unifocal**	**Multifocal**
Lower glands (*n* = 16)	15	5	5	4	2
Upper glands (*n* = 16)	0	2	1	5	8